Prediction of geogrid-reinforced flexible pavement performance using artificial neural network approach[1]

Fan Gu, Ph.D. (Corresponding Author)
Postdoctoral Researcher
National Center for Asphalt Technology
277 Technology Parkway, Auburn, Alabama 36830
Phone: (334) 844-6251, Email: fzg0014@auburn.edu

Xue Luo, Ph.D.
Assistant Research Scientist
Texas A&M Transportation Institute
3135 TAMU, CE/TTI Bldg. 508B, College Station, Texas 77843
Phone: (979) 458-8535, Email: xueluo@tamu.edu

Yuqing Zhang, Ph.D.
Lecturer
School of Engineering and Applied Science
Aston University
MB153A, Aston Triangle, Birmingham, B4 7ET, U.K.
Phone: +44 (0) 121-204-3391, Email: y.zhang10@aston.ac.uk

Yu Chen, Ph.D. Candidate
Graduate Research Assistant
Texas A&M Transportation Institute
3135 TAMU, CE/TTI Bldg. 501J, College Station, Texas 77843
Phone: (979) 676-9382, Email: yu.chen@tamu.edu

Rong Luo, Ph.D., P.E.
Associate Research Engineer
Texas A&M Transportation Institute
3135 TAMU, CE/TTI Bldg. 503C, College Station, Texas 77843
Phone: (979) 845-9897, Email: rongluo@tamu.edu

Robert L. Lytton, Ph.D., P.E.
Professor, Fred J. Benson Chair
Zachry Department of Civil Engineering
Texas A&M University
3136 TAMU, CE/TTI Bldg. 503A, College Station, Texas 77843
Phone: (979) 845-9964, Email: r-lytton@civil.tamu.edu

Prediction of geogrid-reinforced flexible pavement performance using artificial neural network approach

This study aimed to develop a methodology to incorporate geogrid material into the Pavement ME Design software for predicting the geogrid-reinforced flexible pavement performance. A large database of pavement responses and corresponding material and structure properties were generated based on numerous runs of the developed geogrid-reinforced and unreinforced pavement models. The artificial neural network (ANN) models were developed from the generated database to predict the geogrid-reinforced pavement responses. The developed ANN models were sensitive to the change of base and subgrade moduli, and the variation of geogrid sheet stiffness and geogrid location. The ANN model-predicted geogrid-reinforced pavement responses were then used to determine the modified material properties due to geogrid reinforcement. The modified material properties were finally input into the Pavement ME Design software to predict geogrid-reinforced pavement performance. The ANN approach was rapid and efficient to predict geogrid-reinforced pavement performance, which was compatible with the Pavement ME Design software.

Keywords: geogrid-reinforced flexible pavement; finite element model; artificial neural network; pavement ME design

Introduction

Geogrids are widely used by highway agencies to stabilize subgrade soils and reinforce base courses in the construction of flexible pavements. The existing studies indicated that geogrids are effective in improving the stiffness and stability of the reinforced pavements, and reducing the rutting damage (Hass et al., 1988; Al-Qadi et al., 1994; Perkins, 2002; Tang et al., 2015). To extend the use of geogrid in flexible pavement, there is a need to incorporate geogrid material into pavement design. Accurate prediction of geogrid-reinforced flexible pavement performance is a key to pavement design in this respect. The Pavement ME Design software is usually used to predict the flexible pavement performance by taking into account a variety of factors, such as pavement structure, material property, traffic and climate. However, it does not include geogrid material for pavement design (AASHTO, 2008). Thus, it is desirable to develop a methodology to incorporate geogrid material into the Pavement ME Design software, so that the performance of geogrid-reinforced pavements can be accurately predicted. Generally, there are three critical steps involved to achieve this target, which include: a) laboratory characterization of geogrid-reinforced unbound granular material, b) numerical modeling of geogrid-reinforced pavement, and c) prediction of geogrid-reinforced pavement performance using the computed pavement responses.

From the laboratory triaxial tests, geogrids were found to significantly reduce the permanent deformation of unbound granular material (Wayne et al., 2011; Nazzal et al., 2007; Moghaddas-Nejad and Small, 2003; Abu-Farsakh et al., 2007). It was also shown that geogrids did not have any significant influence on enhancing the resilient modulus of large-size unbound aggregates specimens (e.g., 150-mm diameter with 300-mm height, or 200-mm diameter with 400-mm height), but were effective in increasing the resilient modulus of small-size unbound aggregates specimens (e.g., 150-mm

diameter with 200-mm height, or 150-mm diameter with 150-mm height) (Nazzal et al. 2007; Moghaddas-Nejad and Small, 2003; Abu-Farsakh et al., 2007; Rahman et al. 2014; Gu et al., 2016a). Yang and Han (2013) developed an analytical model to quantify the size effect of geogrid reinforcement on the resilient modulus of unbound granular material. The geogrid interlock reinforcement was equivalent to the additional confining stresses that were uniformly distributed on the unbound aggregate specimen. The developed model was capable of predicting the resilient modulus of geogrid-reinforced granular material with different dimensions of specimen, and different material properties of aggregates and geogrids. Gu et al. (2016b) modified the analytical model by replacing the uniform confining stress distribution to the triangular stress distribution. This model improvement took into account the phenomenon that the influence of the geogrid reinforcement decreases with the distance of the aggregates from the geogrid. The modified analytical model successfully predicted both the horizontal and vertical resilient moduli of geogrid-reinforced granular material.

The numerical modeling of geogrid-reinforced pavement mainly tackles the simulation of geogrid reinforcement and geogrid-base/subgrade interface interaction. There are two identified geogrid reinforcement mechanisms, including: a) lateral confinement, which is produced by the interface frictional interaction and interlocking between the base course aggregates and the geogrid layer; and b) vertical membrane effect, which is caused by the vertical membrane deformation to generate an inward shear stress to counteract the outward shear stress induced by the traffic load. Kwon et al. (2005) and Kwon et al. (2008) developed the geogrid-reinforced pavement models using the MATLAB program. They simulated the geogrid lateral confinement by assuming residual stresses or additional confining stresses distributed along the geogrid influence zone, and characterized the geogrid membrane effect by assigning the geogrid

as a membrane element. The nonlinear cross-anisotropic characteristic of granular base was also taken into account in the geogrid-reinforced pavement model. Gu et al. (2016b) improved the geogrid-reinforced pavement models using the ABAQUS software. The analytical model developed by Yang and Han (2013) was used to calculate the additional confining stresses in the geogrid influence zone, which was caused by the geogrid lateral confinement. The interface interaction between geogrid and base/subgrade was defined by the Goodman model. A literature review indicated that another interface model was also used to define the geogrid-base/subgrade interaction, namely Coulomb friction model (Perkins, 2001; Leng and Gabr, 2005). Compared to the Coulomb friction model, the advantage of Goodman model is that the model coefficients can be determined from the pullout test (Luo et al., 2012).

The developed numerical models can accurately compute the critical responses (e.g., critical stresses and strains) of geogrid-reinforced pavement structures subjected to the specified traffic loads. However, these computations are time-consuming and dependent on the commercial finite element software (Ma et al. 2016; Ma et al. 2017). These shortcomings obstacle the direct use of these numerical models for pavement design. The similar problem also occurred to the prediction of reflection or top-down cracking (Lytton et al., 2010; Ceylan et al., 2011; Wu et al., 2014; Ling et al. 2017) and the backcalculation of layer moduli (Meier and Rix, 1994; Ceylan et al., 2005). In these studies, the artificial neural network (ANN) approach was successfully used to link the pavement responses to the material and structure inputs in a quick and easy manner. Thus, the ANN model should also be capable of predicting the geogrid-reinforced pavement responses from any given material and structure properties. An accurate ANN model requires a large database of inputs and outputs. Therefore, it is desirable to generate a database of geogrid-reinforced pavement responses by varying the material

and structure properties. Since the geogrid-reinforced pavement responses are predicted by the ANN models, the performance of geogrid-reinforced pavement can be easily predicted using the distress models in Pavement ME Design.

To achieve this objective, the following tasks were accomplished in this study. First, the numerical modeling of geogrid-reinforced flexible pavements was briefly introduced in the next section, which was elaborated in a previous study (Gu et al., 2016b). Secondly, using the inputs and outputs of the numerical modeling, the subsequent section presented the development of ANN models for predicting the responses of geogrid-reinforced and unreinforced pavements. Thirdly, the method of the modified material properties was proposed to incorporate the ANN results to the Pavement ME Design, so the effect of the geogrid-reinforcement can be included for an arbitrary traffic loading and climate condition. The geogrid-reinforced pavement performance was then predicted by the Pavement ME Design using the computed critical pavement responses from the ANN models. The final section summarized the findings of this paper.

Numerical Modeling of Geogrid-Reinforced Pavement Structures

The finite element models were developed using the ABAQUS software to simulate the geogrid-reinforced flexible pavements (ABAQUS, 2010). Figure 1 illustrated the construction of the finite element meshed geogrid-reinforced pavement model. An axisymmetric geogrid-reinforced pavement model was developed. Fine mesh was used in the vicinity of the load zone. The asphalt concrete, base course and subgrade were represented as 8-node biquadratic homogenous solid elements with reduced integration (Gu et al. 2016c). The geogrid layer was represented by a 3-node quadratic membrane

element. The interface contact between geogrid and base/subgrade was defined by the

Goodman model (Goodman et al., 1968), which was shown in Equation 1.

$$\begin{bmatrix} d\tau \\ d\sigma_n \end{bmatrix} = \begin{bmatrix} k_s & 0 \\ 0 & k_n \end{bmatrix} \begin{bmatrix} du_r \\ dv_r \end{bmatrix} \tag{1}$$

where τ is the shear stress; σ_n is the normal stress; u_r is the relative shear

displacement; v_r is the relative normal displacement; k_s is the shear stiffness; and k_n is

the normal stiffness. The membrane effect of geogrid was characterized by assigning

the geogrid material as a membrane element. The lateral confinement of geogrid was

simulated by assigning the equivalent additional confining stresses in the geogrid-

reinforced zone, which was assumed to be 75-mm thick on both sides of the geogrid

layer (McDowell et al., 2006; Schuettpelz et al., 2009). The detailed procedure for

determining the equivalent additional confining stresses can be found in Gu et al.

(2016b). In the geogrid-reinforced pavement model, the asphalt concrete can be defined

as either the viscoelastic or elastic material. The subgrade layer was defined as the

elastic material. The unbound granular base was characterized as either the nonlinear

stress-dependent cross-anisotropic or linear elastic cross-anisotropic material. The

consideration of cross-anisotropic nature of unbound granular base is important to

accurately predict the pavement responses (Wang and Al-Qadi, 2013; Gu et al., 2015;

Gu et al., 2016d). These settings were in accordance with the hierarchical material input

levels defined in the Pavement ME Design. The prediction accuracy of the developed

models was validated by comparing the model simulation results with the corresponding

large-scale tank test measurements in a previous study (Gu et al., 2016b). It was found

that the simulation results were in good agreement with the large-scale tank test

measurements. This indicated that the developed models were capable of accurately

predicting the geogrid-reinforced pavement responses.

Figure 1

Development of artificial neural network models for predicting geogrid-reinforced pavement responses

The computation of critical pavement responses is the key to forecast the geogrid-reinforced pavement performance. The finite element models shown in the previous section can accurately compute the critical responses of geogrid-reinforced pavements. However, these models were developed using the ABAQUS software, which was not compatible with the Pavement ME Design embedded software DARWin-ME. Furthermore, replacing the current Pavement ME Design software with the developed finite element models to compute the critical responses of the arbitrary user-inputted geogrid-reinforced pavement structures was impractical at the moment. Therefore, there is a need to predict the responses of any given geogrid-reinforced pavement structure based on computation by the developed finite element models for a wide range of geogrid-reinforced pavement structures.

To satisfy this need, the ANN approach was used to predict the critical responses of geogrid-reinforced pavement structures. The ANN models allow establishing the correlations between the input variables X_i and the output variables Y_j through the inter-connected neurons (i.e. weight factor w_{ji}). Herein, the output variables Y_j represented the computed critical pavement responses, including the tensile strain at the bottom of the asphalt concrete, and the compressive strains within the asphalt concrete, base layer and subgrade. The selection of the input parameters X_i was based on the sensitivity analysis of the developed finite element models. The identified input parameters to the ANN model included the layer thickness, the layer modulus, the sheet stiffness of geogrid and the location of geogrid. The correlations developed by the

ANN models between the normalized input parameters x_i and the normalized output

variables y_j were shown in Equation 2.

$$y_j = f\left(\sum_{i=1}^{n} w_{ji} x_i\right) \qquad (2)$$

where f is a transfer function, which normally uses a sigmoidal, Gaussian , or threshold

functional form, and w_{ji} are the unknown weight factors. Developing a neural network

model specifically referred to the determination of the weight factors w_{ji} in Equation 2.

The ANN model determined these weight factors w_{ji} through the two major functions:

training and validating. The training data set was used to determine the trial weight

factors w_{ji}, and the validating data set was employed to examine the accuracy of the

model prediction. A robust ANN model normally requires a large database of input and

output variables. Thus, generating the input and output variables database was the first

step in developing the ANN model.

Experimental Computational Plan for ANN Models

To generate the database, the computation of multiple cases was performed

based on the developed geogrid-reinforced and unreinforced pavement models. Tables

1a and 1b showed the selected input parameters as well as their values for the geogrid-

reinforced pavements and the corresponding unreinforced pavements, respectively.

Based on these experimental computational plans, the number of the computed geogrid-

reinforced pavement models was 2916, and the number of the computed unreinforced

pavement models was 486. From Table 1a, two geogrid locations (i.e., center and

bottom of base course) were taken into account in the computation of the multiple cases.

The pavement responses database is divided into 3 categories, including

- The geogrid placed in the middle of base layer (GG-M),

- The geogrid placed at the bottom of base layer (GG-B), and

- The unreinforced one (Control).

Each category of pavement response database corresponds to one set of neural network models.

Table 1

Development of ANN Models

A three-layered neural network architecture consisting of one input layer, one hidden layer and one output layer was constructed as shown in Figure 2. The input parameters were listed in Table 1, except the geogrid location. The output variables were the critical pavement responses, including the tensile strain at the bottom of asphalt concrete, and the compressive strains within asphalt concrete, base course and subgrade. The hidden layer was assigned 20 neurons to establish the connection between the output layer and the input layer. In this study, the transfer function used a sigmoidal functional form, which was shown in Equation 3 (Ceylan et al., 2014).

$$f(I_i) = \frac{1}{1 + \exp(-\varphi I_i)} \tag{3}$$

where I_i is the input quantity, and φ is a positive scaling constant. The constructed neural network structure was programmed by the software MATLAB 2013a (Demuth and Beale, 1998). The training algorithm used the Levenberg-Marquardt back propagation method to minimize the mean squared error (More, 1978). The gradient descent weight function was employed as a learning algorithm to adjust the weight factors w_{ji} (Amari, 1998).

Figure 2

The pavement response database was first randomly divided into a training data set and a validating data set as the ratio of 80% and 20%, respectively. The training data set was used to determine the weight factors w_{ji}, and the validating data set was employed to examine the prediction accuracy of the developed neural network. Figure 3 showed the comparisons between the finite element model-computed pavement responses and the ANN model-predicted pavement responses for the GG-M structure. It was shown that the ANN model predictions were in good agreement with the finite element model computational results. This indicated that the ANN models accurately predicted all of the pavement responses from the validating data set after the training process. The developed ANN models were used to interpolate the critical responses of any given geogrid-reinforced and unreinforced pavements.

Figure 3

Parametric Study

The sensitivity analysis of the geogrid-reinforced pavement responses predicted by the ANN models was conducted by varying the material properties, such as the base and subgrade moduli, and the sheet stiffness of geogrid. It was found that the primary advantage of geogrid reinforcement was the reduction of the vertical compressive strain in the base course and at the top of subgrade. Therefore, the pavement responses studied in the sensitivity analysis specifically referred to these two critical strains. In this analysis, the flexible pavement consisted of a 100-mm hot mix asphalt (HMA), a 250-mm base course, and semi-infinite subgrade. The geogrid was placed either in the middle or at the bottom of the base course. Table 2 presented the material properties of the control group.

Table 2

Figures 4a and 4b showed the sensitivity of the model-predicted pavement responses to the variation of the subgrade modulus. The selected subgrade moduli were 35 MPa, 70 MPa, 105 MPa and 140 MPa, which represented the poor, fair, good and very good quality of subgrade, respectively. The increase of subgrade modulus remarkably decreased the vertical strain at the top of subgrade, but slightly increased the vertical strain within the base layer. The placement of the geogrid was effective in reducing these two critical strains. The reduction of the critical strains due to the geogrid reinforcement were normalized using Equation 4.

$$Normalized\ reduction\ of\ strain = \frac{Strain\_Control - Strain\_Geogrid}{Strain\_Control} \times 100\% \quad (4)$$

where $Strain\_Control$ is the computed critical strain in the control model, $Strain\_Geogrid$ is the computed critical strain in the geogrid-reinforced model. Figure 4c indicated that the reduction of the vertical strain at the top of subgrade was significant when the geogrid was placed at the bottom of the base course. The increase of subgrade modulus slightly decreased the reduction percentage by the presence of geogrid. Figure 4d illustrated that the geogrid reinforced in the middle of the base course was more effective in reducing the vertical strain of base layer than that placed at the base/subgrade interface. The normalized reduction of the base vertical strain due to geogrid reinforcement decreased with the increase of subgrade modulus. This indicated that the geogrid reinforcement was more effective when it was placed over a weak subgrade, which normally had a low resilient modulus.

Figure 4

Figures 5a and 5b presented the sensitivity of the model-predicted pavement responses to the variation of the base modulus. The selected base moduli were 140 MPa, 210 MPa, 280 MPa and 350 MPa, which were used to represent the various

quality of base course. It was found that the increase of base modulus effectively reduced the vertical strain in both base layer and subgrade. Figures 5c and 5d showed the normalized reduction of critical strains corresponding to the different base modulus. The effect of geogrid location on pavement responses was in accordance with the findings from Figures 4c and 4d. The normalized reduction of vertical strain in base decreased with the increase of base modulus, while the normalized reduction of vertical strain at the top of subgrade increased with the increase of base modulus. This demonstrated that the geogrid placed in the middle of base course was more effective for a weak base course, and the geogrid placed at the base/subgrade interface was more effective for a strong base course.

Figure 5

Figures 6a and 6b showed the sensitivity of the pavement responses predicted by the model to the variation of the geogrid sheet stiffness. Both the vertical strain at the top of subgrade and the average vertical strain within the base layer decreased with the increase of the geogrid sheet stiffness. This indicated that the geogrid with a higher sheet stiffness was more efficient in reducing the rutting damage of flexible pavements.

Figure 6

Prediction of Geogrid-Reinforced Pavement Performance

The performance of geogrid-reinforced flexible pavements includes fatigue cracking, permanent deformation and international roughness index (IRI). The aforementioned ANN model-predicted critical pavement responses can be used to predict the pavement performance using the distress models in the current Pavement ME Design. However, this method ignored the influence of traffic and climate on the pavement performance.

To eliminate this defect, the material properties of geogrid-reinforced pavement structure were first equivalent to a combination of modified material properties (e.g., modified base modulus and modified subgrade modulus) of an unreinforced pavement structure. The determined modified material properties were then input into the Pavement ME Design software to predict the pavement performance. Using this approach, the influence of traffic and climate on the pavement performance were taken into account by the Pavement ME Design software.

Determination of Modified Material Properties

Figure 7 presented a flowchart to determine the modified material properties for a geogrid-reinforced pavement. When a user inputs the geogrid-reinforced pavement information (e.g., layer thickness and material properties), the program will automatically generate a control structure with the same layer thickness and material properties. The ANN models are utilized to predict the responses of the geogrid-reinforced and the control pavement structures. Subsequently, the responses of the geogrid-reinforced pavement structure are compared to those of the control structure. Equation 5 presented the convergence criteria used in this flowchart.

$$\frac{\left|\varepsilon_{geogrid} - \varepsilon_{control}\right|}{\varepsilon_{control}} \leq 10\% \tag{5}$$

where $\varepsilon_{geogrid}$ represents the response of the geogrid-reinforced pavement structure, and $\varepsilon_{control}$ represents the response of the control structure. If the responses of geogrid-reinforced pavement structure do not match those of the control structure, the material properties (i.e., base material and subgrade modulus) of the control structure should be modified. The iteration will end till the comparison of the critical responses passes the convergence criteria. The program then outputs the modified material properties of the

control structure, which are the inputs of the Pavement ME Design software. The

program was written using C# language, which was compatible with the current

Pavement ME Design software.

Figure 7

Case studies were performed on the same flexible pavement structures used in

the parametric study. The material properties of the geogrid-reinforced pavements were

shown in Table 2. The modified material properties of the control pavement structure

were determined using the aforementioned approach, as presented in Figure 8. It was

shown that placing the geogrid in the middle or at the bottom of base course was

equivalent to increasing the moduli of base course and subgrade.

Figure 8

Prediction of Pavement Performance

The pavement structures in the case studies were assumed to be constructed in

College Station, Texas. The two-way average annual daily truck traffic was 2000. The

vehicle class distribution and growth followed the default values of Pavement ME

Design. The climate information was collected from the weather station in College

Station, Texas. The Pavement ME Design software was used to predict the performance

of geogrid-reinforced and unreinforced pavements. Figure 9 showed the effect of

geogrid location on the flexible pavement performance. In Figure 9a, the least amount

of fatigue cracking occurred with the geogrid placed at the bottom of the base course,

slightly outperforming the unreinforced pavement section. This indicated that placing

the geogrid in the center of the base course slightly reduced the fatigue life of flexible

pavement. Figure 9b presented the effect of geogrid location on rutting damage of

flexible pavement. Compared to the control pavement, placing the geogrid in the center or at the bottom of the base course effectively reduced the accumulated permanent deformation of flexible pavement. The least amount of rutting damage occurred with the geogrid placed at the bottom of the base course. In Figure 9c, the pavement with the lowest IRI emerged as the one with the geogrid at the bottom of the base course. These example calculations indicated that the major benefit of geogrid to the performance of flexible pavements was derived from a reduction of rutting and roughness. In these case studies, the placement of a geogrid at the bottom of the base course achieved the most beneficial effect.

Figure 9

Summary and Conclusions

This study developed an artificial neural network (ANN) approach to predict the geogrid-reinforced flexible pavement performance. The major contributions of this paper were summarized as follows:

- The finite element modeling of geogrid-reinforced pavements took into account the two geogrid reinforcement mechanisms, i.e., the lateral confinement and the membrane effect. Based on a large number of runs of these finite element models, the ANN models were developed to rapidly predict the geogrid-reinforced pavement responses.

- The placement of the geogrid was effective in reducing the vertical compressive strain in base course and at the top of subgrade. The reduction of the vertical strain at the top of subgrade was significant (e.g., 40%-50%) when the geogrid was placed at the bottom of the base course. The geogrid reinforced in the middle of the base course effectively (e.g., 8%-10%) reduced the average vertical strain of base course.

- The geogrid reinforcement was more effective when it was placed over a weak subgrade, which normally had a low resilient modulus. The geogrid placed in the middle of base course was more effective for a weak base course, and the geogrid placed at the base/subgrade interface was more effective for a strong base course. The geogrid with a higher sheet stiffness was more efficient in reducing the rutting damage of flexible pavement.

- Using a pavement response-based method, the material properties of geogrid-reinforced pavement structure were equivalent to a combination of modified material properties (e.g., modified base modulus and modified subgrade modulus) of an unreinforced pavement structure. The modified material properties were input into the Pavement ME Design software to successfully predict the geogrid-reinforced pavement performance. The proposed ANN approach was programmed using C# language, which was compatible with the current Pavement ME Design software.

In the future, the ANN computational plan will be expanded to cover a wider range of material properties and structure data (e.g., layer thickness and geogrid location). The field performance data will be collected to calibrate and validate the current performance prediction models.

Acknowledgment

Disclosure statement

No potential conflict of interest was reported by the authors.

Funding

References

AASHTO. (2008). Mechanistic-empirical pavement design guide: a manual of practice, interim edition. American Association of State Highway and Transportation Officials, Washington DC.

ABAQUS. (2010). ABAQUS standard user's manual. Abaqus Inc., Providence, RI.

Abu-Farsakh, M. Y., Nazzal, M. D., and Mohammad, L. N. (2007). Effect of reinforcement on resilient and permanent deformations of base course material. *Transportation Research Record: Journal of Transportation Research Board*, 2004(1), 120-131.

Al-Qadi, I. L., Brandon, T. L., Valentine, R. J., Lacina, B. A., and Smith, T. E. (1994). Laboratory evaluation of geosynthetic-reinforced pavement sections. *Transportation Research Record: Journal of Transportation Research Board*, 1439(1), 25-31.

Amari, S. (1998). Natural gradient works efficiently in learning. *Neural Computation*, 10(2), 251-276.

Ceylan, H., Guclu, A., Tutumluer, E., and Thompson, M. R. (2005). Backcalculation of full-depth asphalt pavement layer moduli considering nonlinear stress-dependent subgrade behavior. *International Journal of Pavement Engineering*, 6(3), 171-182.

Ceylan, H., Gopalakrishnan, K., and Lytton, R. L. (2011). Neural networks modeling of stress growth in asphalt overlays due to load and thermal effects during reflection cracking. *Journal of Materials in Civil Engineering*, 23(3), 221-229.

Ceylan, H., Bayrak, M. B., and Gopalakrishnan, K. (2014). Neural networks applications in pavement engineering: a recent survey. *International Journal of Pavement Research and Technology*, 7(6), 434-444.

Demuth, H., and Beale, M. (1998). Neural network toolbox for use with MATLAB. The MathWorks, Natick, MA.

Goodman, R. E., Taylor, R. L., and Brekke, T. L. (1968). A model for the mechanics of jointed rock. *Journal of the Soil Mechanics and Foundations Division*, 94(3), 637-660.

Gu, F., Sahin, H., Luo, X., Luo, R., and Lytton, R. L. (2015). Estimation of resilient modulus of unbound aggregates using performance-related base course properties. *Journal of Materials in Civil Engineering*, 27(6), 04014188.

Gu, F., Zhang, Y., Luo, X., Luo, R., and Lytton, R. L. (2016a). Impact of geogrid on cross-anisotropy and permanent deformation of unbound granular materials. *Transportation Research Record: Journal of the Transportation Research Board*, 2580(1), 34-46.

Gu, F., Luo, X., Luo, R., Lytton, R. L., Hajj, E. Y., and Siddharthan, R. V. (2016b). Numerical modeling of geogrid-reinforced flexible pavement and corresponding validation using large-scale tank test. *Construction and Building Materials*, 122, 214-230.

Gu, F., Luo, X., Zhang, Y., Lytton, R. L., and Sahin, H. (2016c). Modeling of unsaturated granular materials in flexible pavements. *E3S Web of Conferences*, 9, 20002.

Gu, F., Zhang, Y., Droddy, C. V., Luo, R., and Lytton, R. L. (2016d). Development of a new mechanistic-empirical rutting model for unbound granular material. *Journal of Materials in Civil Engineering*, 28(8), 04016051.

Hass, R., Walls, J., and Carroll, R. G. (1988). Geogrid reinforcement of granular bases in flexible pavements. *Transportation Research Record: Journal of Transportation Research Board*, 1188(1), 19-27.

Kwon J., Tutumluer, E., and Kim, M. (2005). Development of a mechanistic model for geosynthetic-reinforced flexible pavements. *Geosynthetics International*, 12(6), 310-320.

Kwon J., Tutumluer, E., and Konietzky, H. (2008). Aggregate base residual stresses affecting geogrid reinforced flexible pavement response. *International Journal of Pavement Engineering*, 9(4), 275-285.

Leng, J., and Gabr, M. A. (2005). Numerical analysis of stress-deformation response in reinforced unpaved road sections. *Geosynthetics International*, 12(2), 111-119.

Ling, M., Luo, X., Hu, S., Gu, F., and Lytton, R. L. (2017). Numerical modeling and artificial neural network for predicting J-integral of top-down cracking in asphalt concrete pavement. Transportation Research Record, 2631(1), in press.

Luo, R., Gu, F., and Lytton, R. L. (2012). Quantifying the influence of geosynthetics on pavement performance. *NCHRP Project 1-50 Interim Report*, National Cooperative Highway Research Program, Transportation Research Board, Washington, DC.

Lytton, R. L. Tsai, F. L., Lee, S. I., Luo, R., Hu, S., and Zhou, F. (2010). Models for predicting reflection cracking of hot-mix asphalt overlays. *NCHRP Report 669*, National Cooperative Highway Research Program, Transportation Research Board, Washington, DC.

Ma, T., Zhang, D., Zhang, Y., Hong, J. (2016). Micromechanical response of aggregate skeleton with asphalt mixture based on virtual simulation of wheel tracking test. Construction and Building Materials, 111, 153-163.

Ma, T., Wang, H., Zhang, D., and Zhang, Y. (2017). Heterogeneity effect of mechanical property on creep behavior of asphalt mixture based micromechanical modeling and virtual creep test. Mechanics of Materials, 104, 49-59.

McDowell, G. R., Harireche, O., Konietzky, H., Brown, S. F., and Thom, N. H. (2006). Discrete element modelling of geogrid-reinforced aggregates. *Proceedings of the Institution of Civil Engineers: Geotechnical Engineering*, 159(1), 35-48.

Meier, R. W., and Rix, G. J. (1994). Backcalculation of flexible pavement moduli using artificial neural networks. *Transportation Research Record: Journal of the Transportation Research Board*, 1448(1), 75-82.

Moghaddas-Nejad, F., and Small, J. C. (2003). Resilient and permanent characteristics of reinforced granular materials by repeated load triaxial tests. *Geotechnical Testing Journal*, 26(2), 152-166.

More, J. (1978). The Levenberg-Marquardt algorithm: implementation and theory. *Numerical Analysis*, 630, 105-116.

Nazzal, M., Abu-Farsakh, M., and Mohammad, L. (2007). Laboratory characterization of reinforced crushed limestone under monotonic and cyclic loading. *Journal of Materials in Civil Engineering*, 19(9), 772-783.

Perkins, S. W. (2001). Mechanistic-empirical modeling and design model development of geosynthetic reinforced flexible pavements. *Report No. FHWA/MT-01/002/99160-1A*, 156p.

Perkins, S. W. (2002). Evaluation of geosynthetic reinforced flexible pavement systems using two pavement test facilities. *Report No. FHWA/MT-02-008/20040*, 120p.

Rahman, M., Arulrajah, A., Piratheepan, J., Bo, M., and Imteaz, M. (2014). Resilient modulus and permanent deformation responses of geogrid-reinforced construction and demolition materials. *Journal of Materials in Civil Engineering*, 26(3), 512-519.

Schuettpelz, C., Fratta, D., and Edil, T. B. (2009). Evaluation of the zone of influence and stiffness improvement from geogrid reinforcement in granular materials.

Transportation Research Record: Journal of the Transportation Research Board, 2116(1), 76-84.

Tang, X., Palomino, A. M., and Stoffels, S. M. (2016). Permanent deformation behavior of reinforced flexible pavements built on soft soil subgrade. *Road Materials and Pavement Design*, 17(2), 311-327.

Wang, H., and Al-Qadi, I. (2013). Importance of nonlinear anisotropic modeling of granular base for predicting maximum viscoelastic pavement responses under moving vehicular loading. *Journal of Engineering Mechanics*, 139(1), 29-38.

Wayne, M., Boudreau, R. L., and Kwon, J. (2011). Characterization of mechanically stabilized layer by resilient modulus and permanent deformation testing. *Transportation Research Record: Journal of the Transportation Research Board*, 2204(1), 76-82.

Wu Z., Hu, S., and Zhou, F. (2014). Prediction of stress intensity factors in pavement cracking with neural networks based on semi-analytical FEA. *Expert Systems with Applications*, 41(4), 1021-1030.

Yang, X., and Han, J. (2013). Analytical model for resilient modulus and permanent deformation of geosynthetic-reinforced unbound granular material. *Journal of Geotechnical and Geoenvironmental Engineering*, 139(9), 1443-1453.

List of Tables and Figures

Table 1. Selected Input Parameters for Model Computation

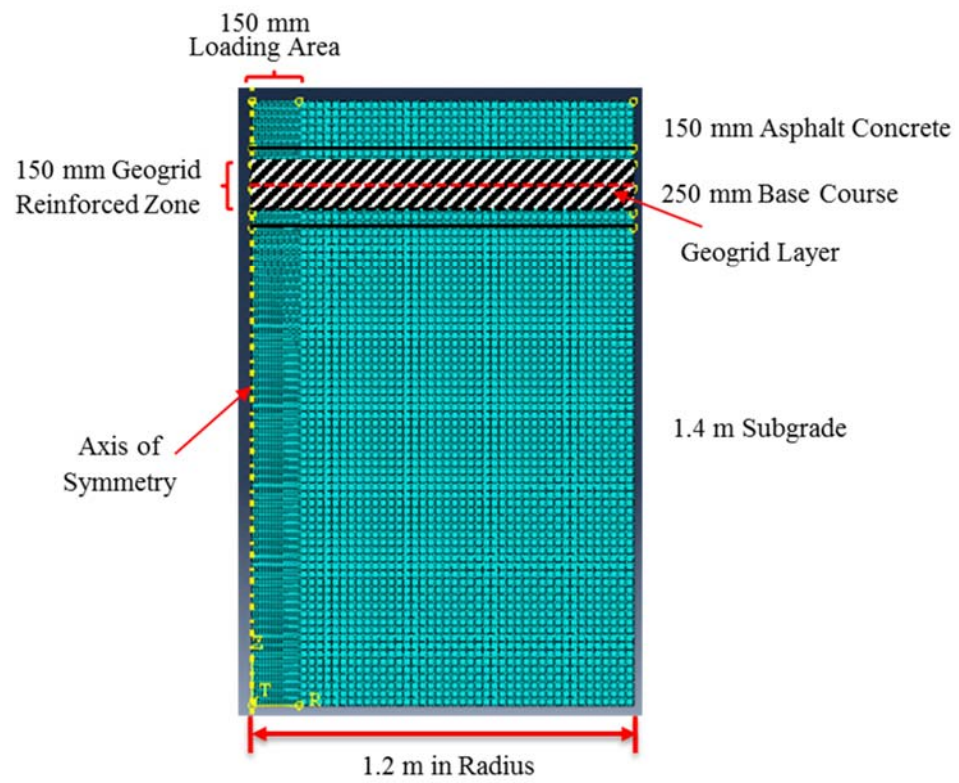Table 2. Material Properties of Geogrid-Reinforced Pavements for Case Studies

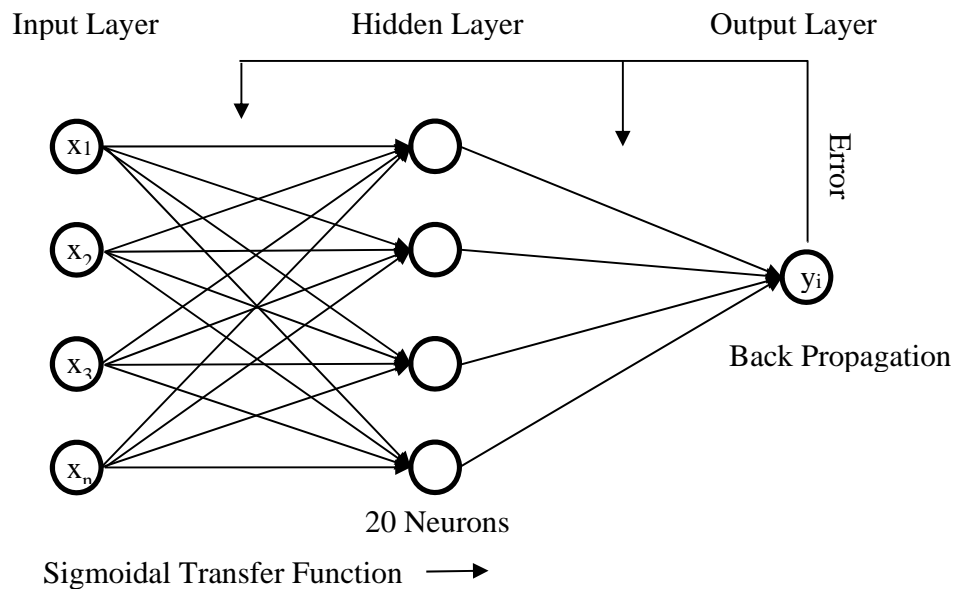Figure 1. Finite Element Meshed Geogrid-Reinforced Pavement Model

Figure 2. Illustration of Three-Layered Neural Network Architecture

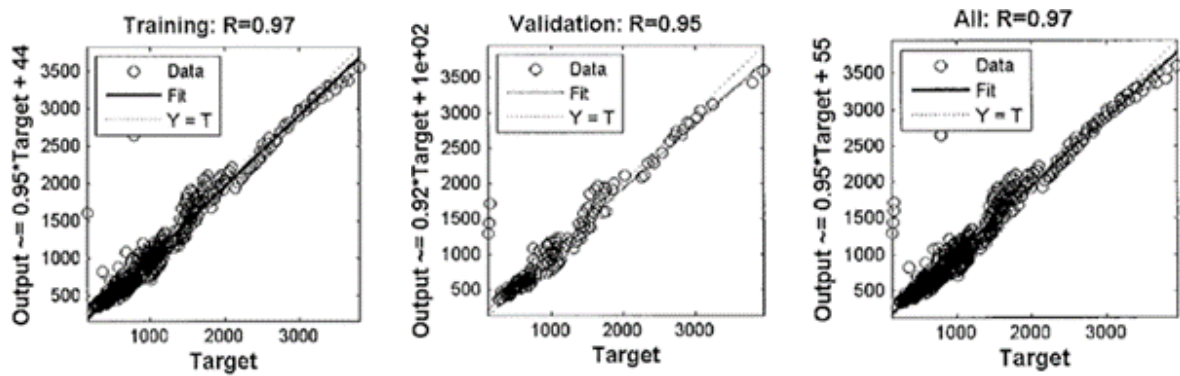Figure 3. Comparison of Critical Responses between Finite Element Model Computations and ANN Model Predictions

Figure 4. Sensitivity of Model-Predicted Pavement Responses to Subgrade Modulus

Figure 5. Sensitivity of Model-Predicted Pavement Responses to Base Modulus

Figure 6. Sensitivity of Model-Predicted Pavement Responses to Geogrid Sheet Stiffness

Figure 7. Process of Predicting Geogrid-Reinforced Pavement Performance

Figure 8. Determination of Modified Material Properties

Figure 9. Effect of Geogrid Location on Pavement Performance

TABLE 1 Selected Input Parameters for Model Computation

(a) Selected Input Parameters for Geogrid-Reinforced Pavements

Influential Factors	Level	Input Values
Load Magnitude	1	565 kPa
HMA Thickness	3	5, 10, and 15 cm
HMA Modulus	3	2100, 3150 and 4200 MPa
Base Thickness	3	15, 25, and 38 cm
Base Vertical Modulus	3	140, 280 and 420 MPa
Base Anisotropic Ratio	2	0.35 and 0.45
Geogrid Location	2	Center and Bottom of Base Course
Geogrid Sheet Stiffness	3	210, 420 and 630 kN/m
Subgrade Modulus	3	35, 105 and 175 MPa
The Number of Total Cases is 2916.		

(b) Selected Input Parameters for Unreinforced Pavements

Influential Factors	Level	Input Values
Load Magnitude	1	565 kPa
HMA Thickness	3	5, 10, and 15 cm
HMA Modulus	3	2100, 3150 and 4200 MPa
Base Thickness	3	15, 25, and 38 cm
Base Vertical Modulus	3	140, 280 and 420 MPa
Base Anisotropic Ratio	2	0.35 and 0.45
Subgrade Modulus	3	35, 105 and 175 MPa

The Number of Total Cases is 486.

TABLE 2 Material Properties of Geogrid-Reinforced Pavements for Case Studies

Material Type	Thickness (mm)	Vertical Modulus (MPa)	Anisotropic Ratio	Sheet Stiffness (kN/m)	Poisson's Ratio
HMA	100	2100	N/A[a]	N/A	0.35
Base Course	250	210	0.4	N/A	0.4
Subgrade	N/A	70	N/A	N/A	0.4
Geogrid	2	N/A	N/A	420	0.3

a. N/A = Not Available

FIGURE 1 Finite element meshed geogrid-reinforced pavement model.

FIGURE 2 Illustration of three-layered neural network architecture.
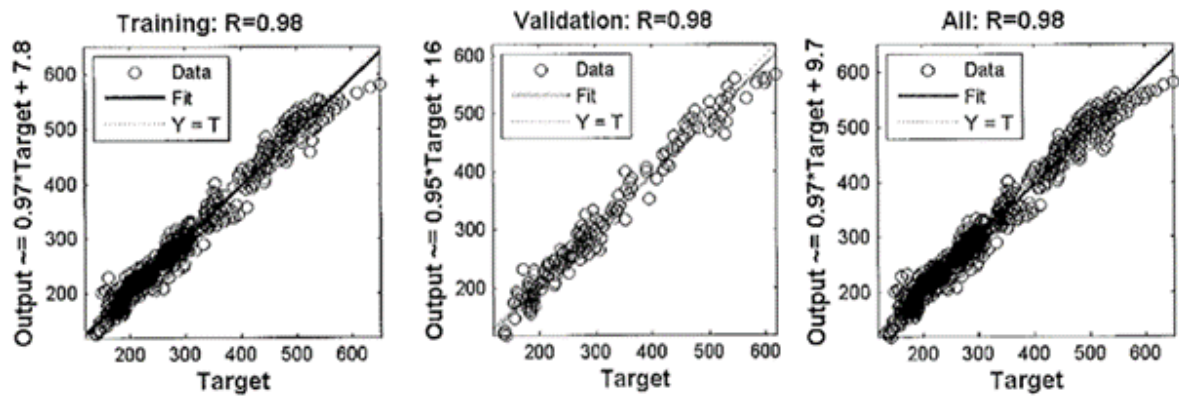
a. Tensile Strain at the Bottom of the Asphalt Concrete
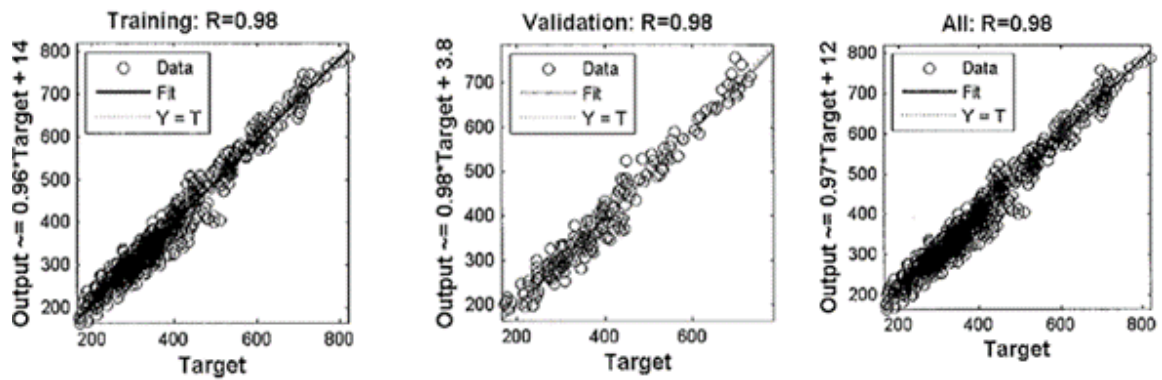
b. Average Vertical Strain in the Asphalt Concrete
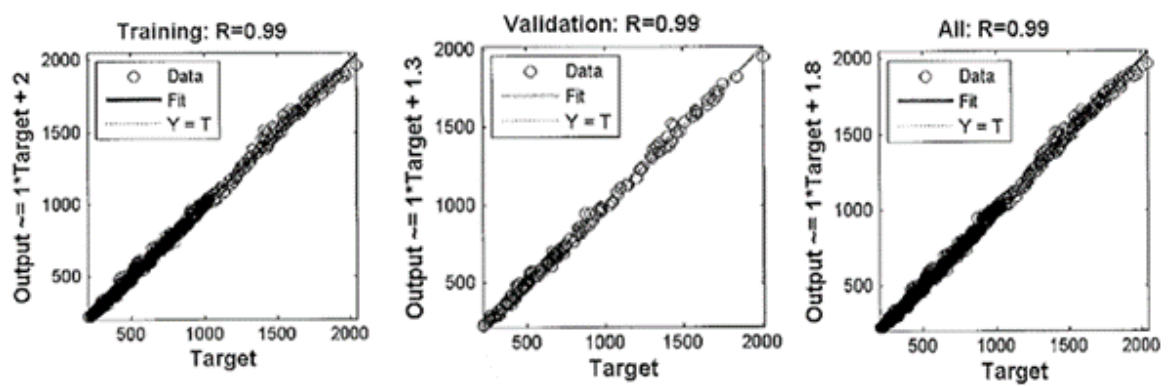
c. Average Vertical Strain in the Base Layer

d. Vertical Strain at the Top of the Subgrade
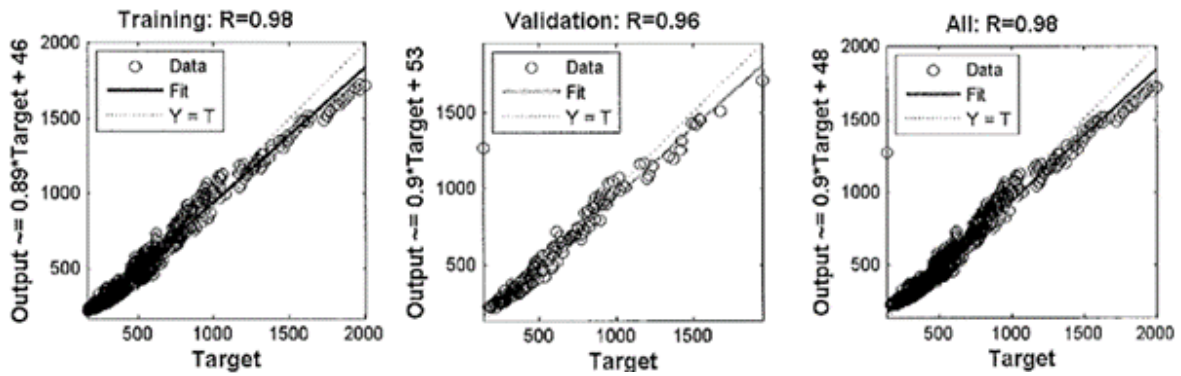
e. Vertical Strain at 150 mm below the Top of the Subgrade

FIGURE 3 Comparison of critical responses between finite element model computations and ANN model predictions.
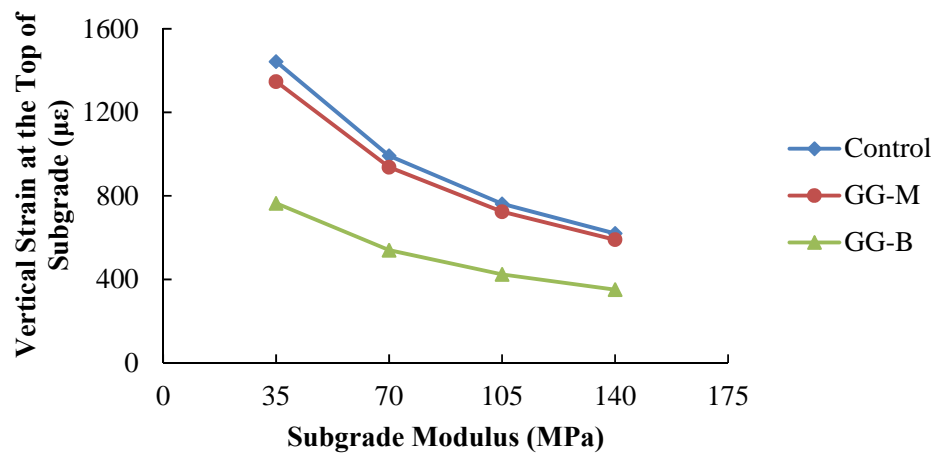
a. Computed Vertical Strain at the Top of Subgrade
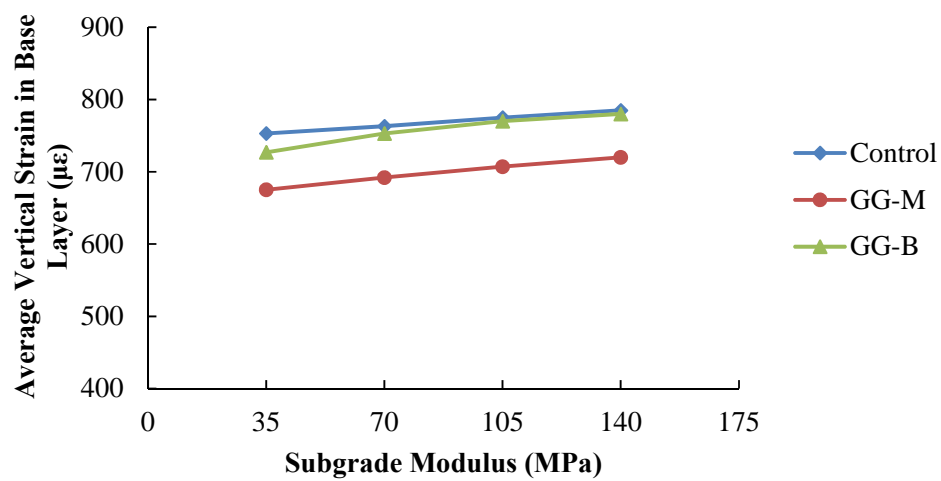
b. Computed Average Vertical Strain in Base Layer
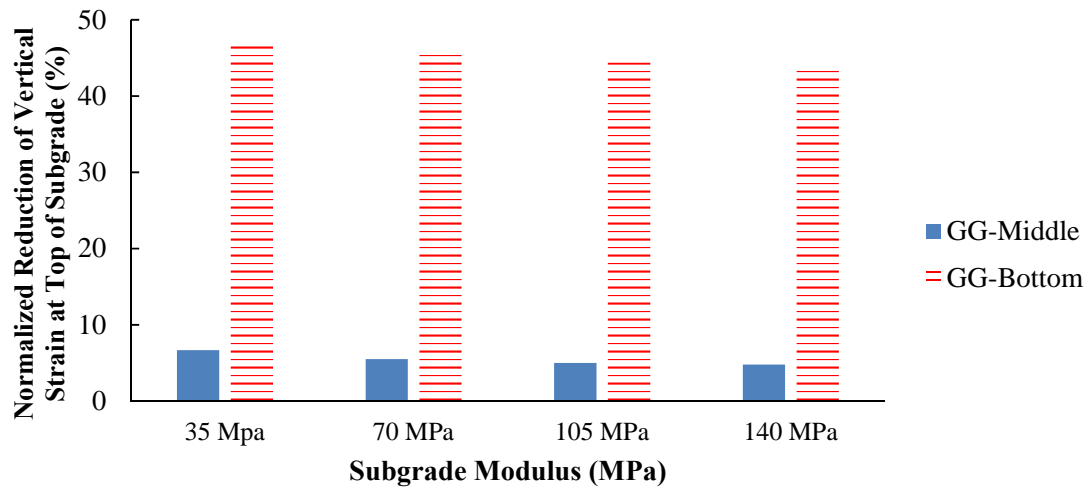
**c. Normalized Reduction of Vertical Strain at the Top of Subgrade**
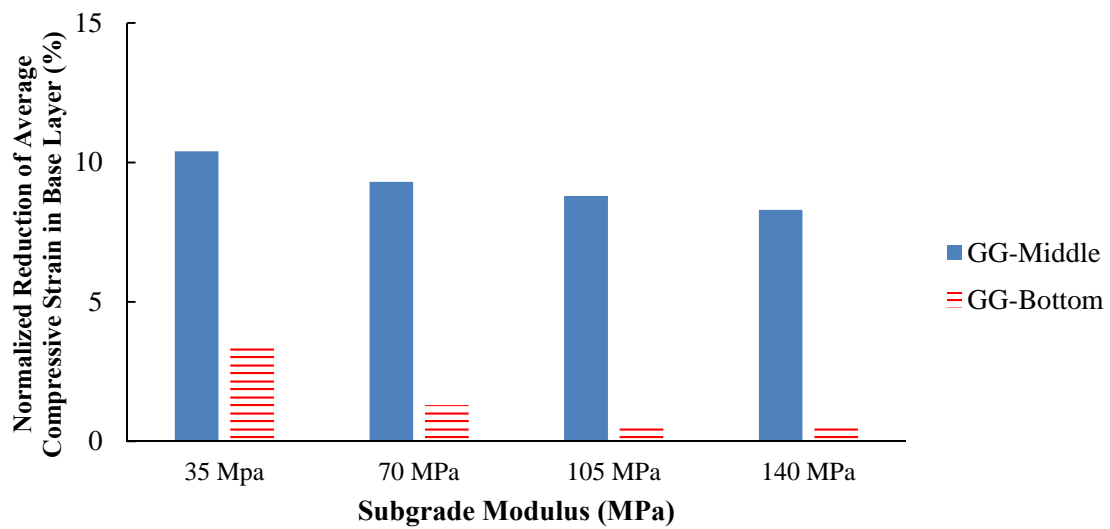
d. Normalized Reduction of Average Vertical Strain in Base Layer

FIGURE 4 Sensitivity of model-predicted pavement responses to subgrade modulus.
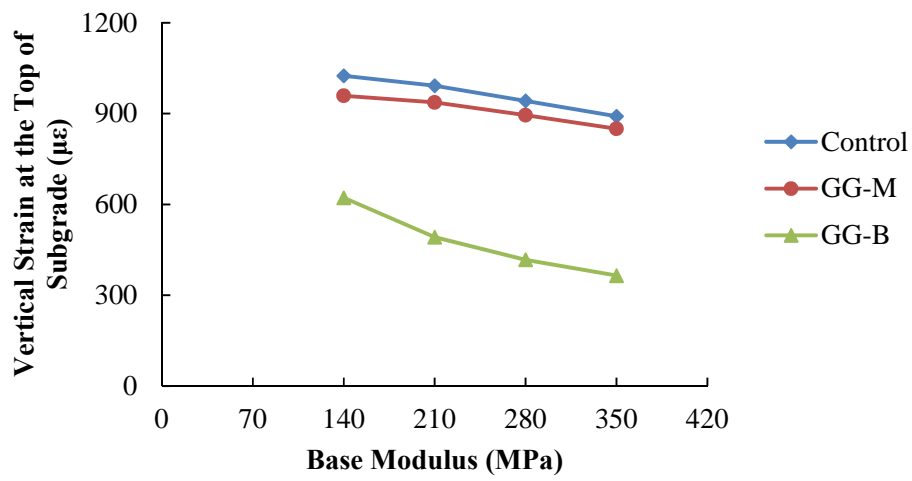
a. Computed Vertical Strain at the Top of Subgrade
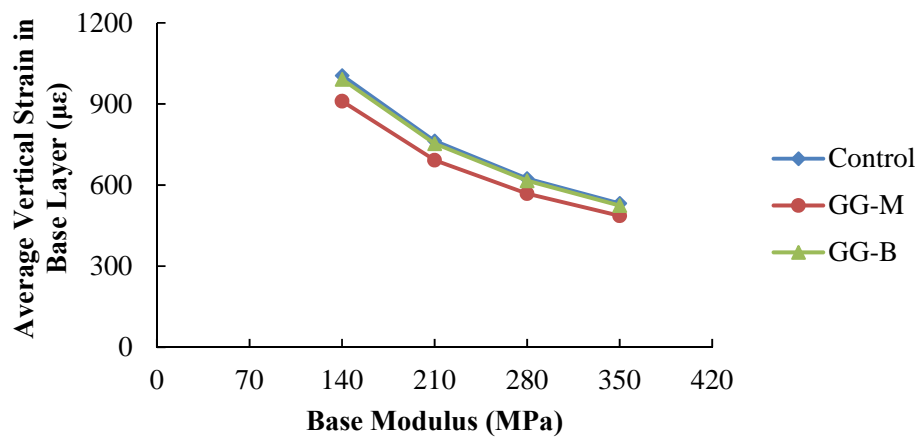
b. Computed Average Vertical Strain in Base Layer
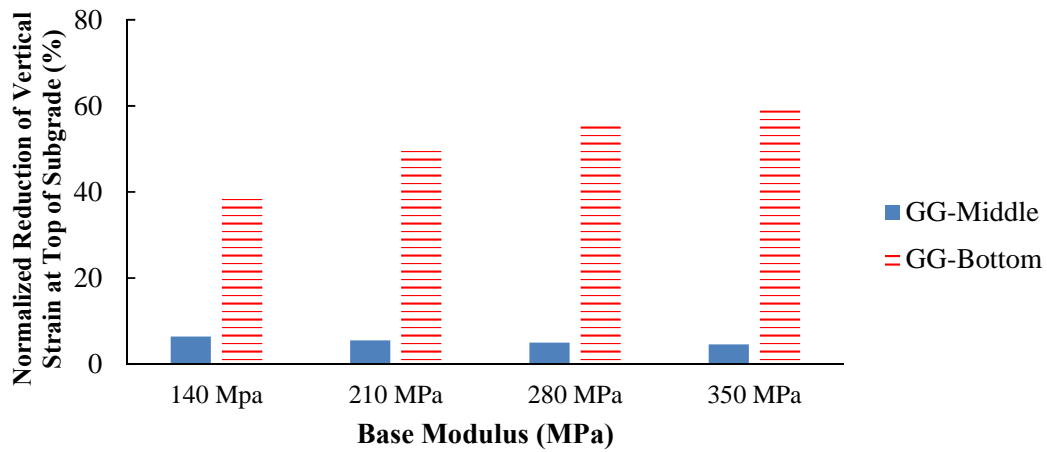
c. Normalized Reduction of Vertical Strain at the Top of Subgrade
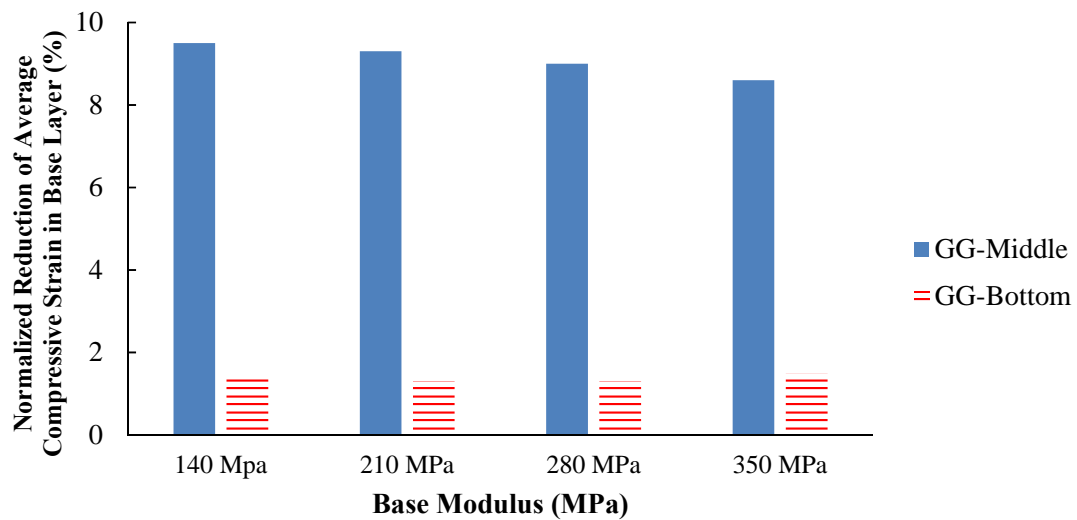
d. Normalized Reduction of Average Vertical Strain in Base Layer

FIGURE 5 Sensitivity of model-predicted pavement responses to base modulus.
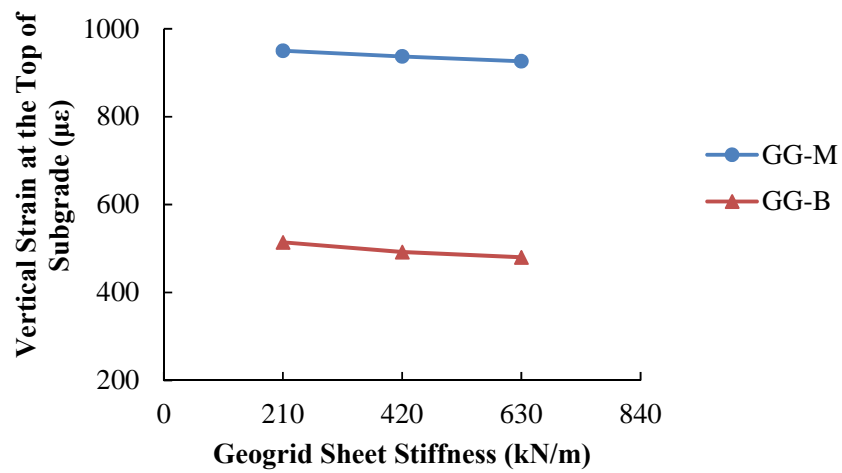
a. Computed Vertical Strain at the Top of Subgrade
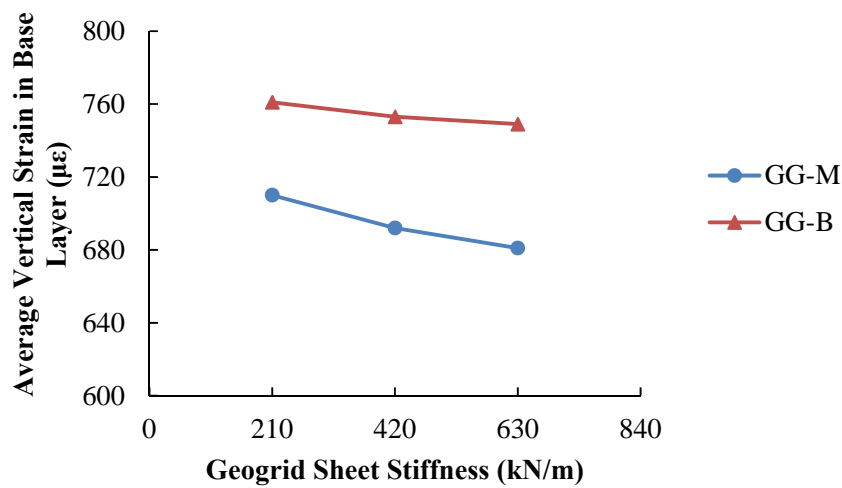
b. Computed Average Vertical Strain in Base Layer

FIGURE 6 Sensitivity of model-predicted pavement responses to geogrid sheet stiffness.
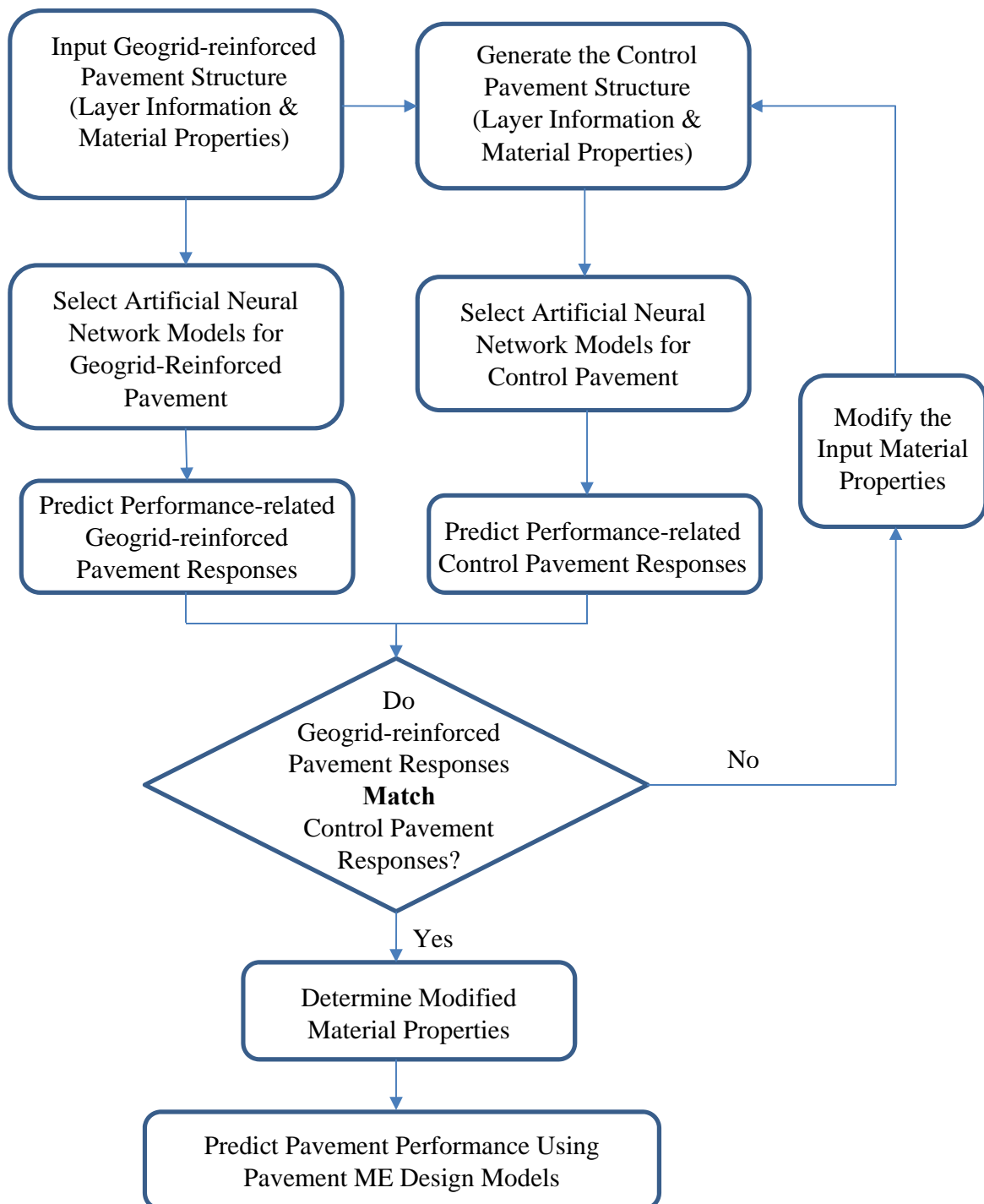
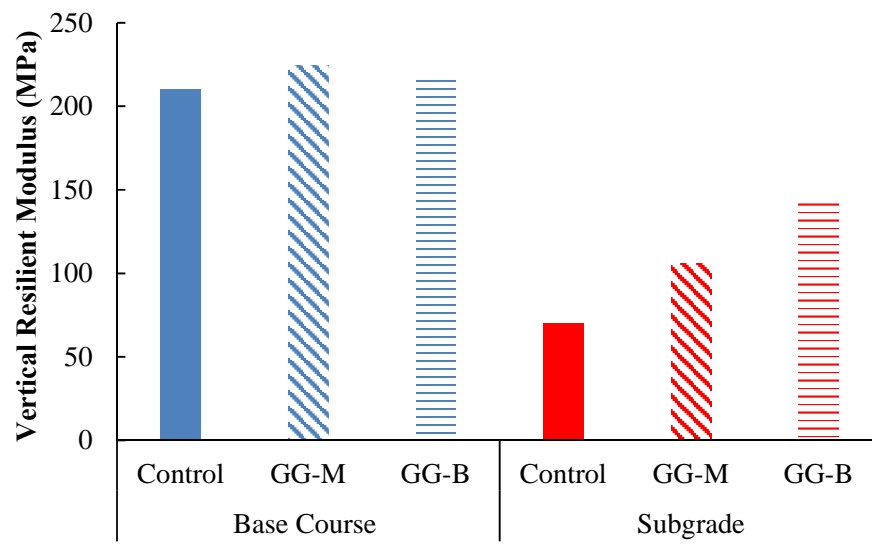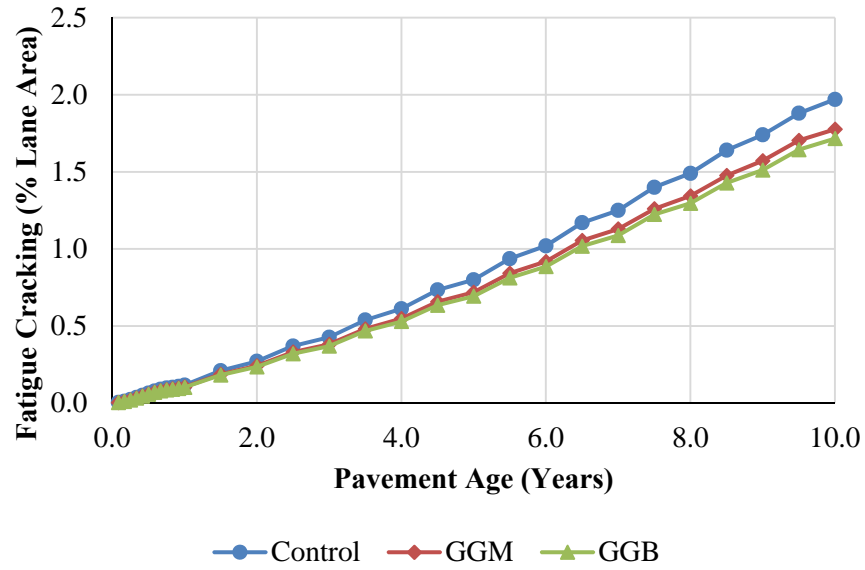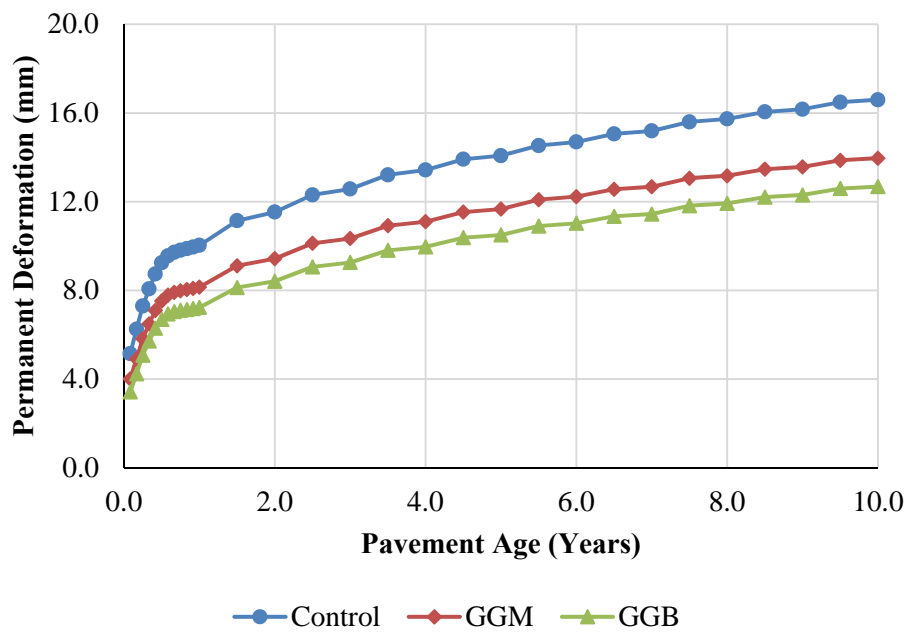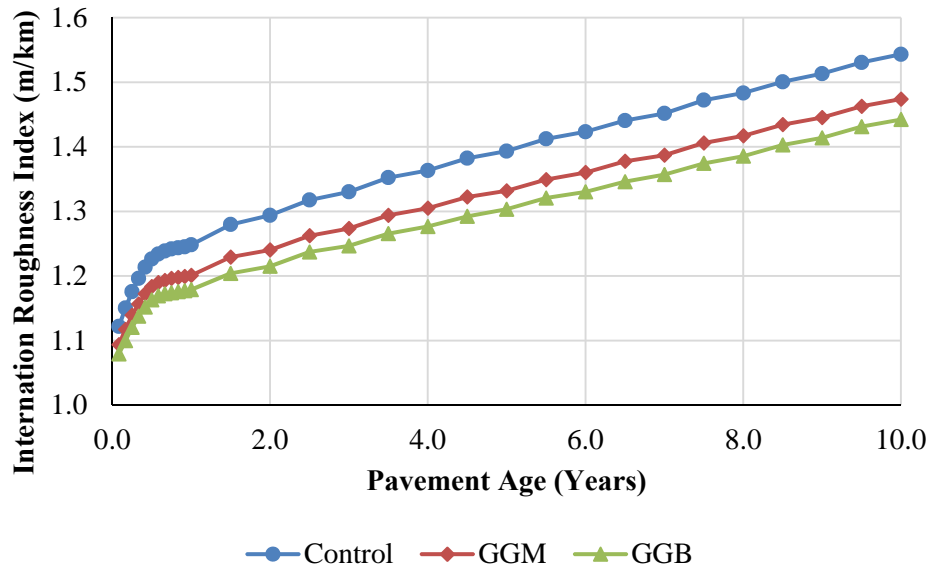**FIGURE 7 Process of predicting geogrid-reinforced pavement performance.**

FIGURE 8 Determination of modified material properties.

a. Effect of Geogrid Location on Fatigue Cracking

b. Effect of Geogrid Location on Rutting Depth

c. Effect of Geogrid Location on IRI

FIGURE 9 Effect of geogrid location on pavement performance.